Reduction of Dichlorosiliane-Based Tungsten Silicide Resistivity by Amorphization and Its Applicability as an Electrode

Jeong Soo Byun,[a,*,c] Byung Hak Lee,[a] Ji-Soo Park,[a] Dong Kyun Sohn,[a] Jeongeui Hong,[b] Won-Ju Cho,[b] Sang Jun Choi,[a] and Jae Jeong Kim[a]

LG Semicon Company, Limited, [a]Research and Development Division, [b]MemoryBusiness HQ, Hungduk-gu, Cheongju-si 361-480, Korea

The impact of ion implantation on dichlorosilane-based tungsten silicide is reported with an emphasis on structural changes and the formation of low-resistivity silicide. It was found that implantation to the as-deposited dichlorosilane-based tungsten layer with the hexagonal close-packed structure resulted in amorphization. After thermal annealing for crystallization, the amorphized silicide was converted to the large-grain-sized tetragonal structure in which the resistivity of the silicide was about 30% lower than that of the conventional structure. In addition, the surface of the implanted silicide was smoother than that of the conventional one. The resistivity after thermal activation depended on the implantation conditions: implantation species, energy, and dose. Among all implantation species tested, phosophorus ions were found to be the most effective in terms of device fabrication. For optimized device performance, the energy should be controlled to contain the ions in the silicide. With this condition, device performance was not adversely affected, and line resistance and dopant depletion were improved.
© 1999 The Electrochemical Society. S0013-4651(98)06-032-7. All rights reserved.

The most common low-resistance, high-melting-point metallization material in current semiconductor devices is polycide, which is defined as a silicide over doped polycrystalline silicon (poly-Si). Due to its excellent thermal stability and fabrication compatibility, tungsten polycide (WSi_x/poly-Si) gate and bit line interconnects are well established in very-large-scale integrated circuit (VLSI) applications. Studies have been reported on the chemical vapor deposition (CVD) of WSi_x using SiH_4 and WF_6 or SiH_2Cl_2 [dichlorosilane (DCS)] and WF_6 chemistries, which are termed the silane-based WSi_x (SiH_4-WSi_x)[1-4] and the DCS-based WSi_x (DCS-WSi_x) process,[5-10] respectively. Recent work has shown that DCS-WSi_x are of high quality with less particluates, better confirmality of step coverage, and lower fluorine incorporation in comparison with SiH_4-WSi_x films. It is known that the higher deposition temperature of DCS-WSi_x causes crystallization of the film during deposition to hexagonal close-packed WSi_2, a low-temperature polymorphism of tungsten silicide (termed hcp-WSi_2).[11,12] Following thermal treatment, the crystallinity of the as-deposited silicide restricts the recrystallization to the tetragonal structured WSi_2, a high-temperature polymorphism of tungsten silicide (termed tet-WSi_2).[13] Due to such an effect, the minimum resistivity of the silicide is around 100 $\mu\Omega$ cm after thermal annealing,[14] which is too high for the polycide to be successfully used in future complementary metal-oxide-semiconductor (CMOS) devices.

In the transition from megabit to gigabit-scale dynamic random memory (DRAM), many efforts have been made to replace the tungsten polycide by lower resistivity materials. For example, tungsten (W)[15-17] and titanium polycide ($TiSi_x$/poly-Si) gates[18,19] were recently reported to be attractive because of their lower resistivities, around 10 and 15 $\mu\Omega$ cm, respectively. Unfortunately, however, process issues which may arise during device fabrication, such as particle contamination, cleaning processes, feasible diffusion barriers, and thermal stability, have not been fully evaluated. Thus, a detailed study is required for these processes to be efficiently applied in a manufacturing environment.

As one of the solutions, the present authors suggested an integrated cluster process of the polycide[14] and reported its successful use in a gigabit-scale DRAM.[20] The main argument of the process was based on the formation of amorphous-phase tungsten silicide layer by the dopant (i.e., phosphorus) reduction phenomenon.[10] During the following thermal treatment, large-sized grains of tet-WSi_2 are formed with resistivities less than 40 $\mu\Omega$ cm. However, this process is limited to certain equipment configurations due to its sequential deposition of the doped poly-Si and the DCS-WSi_x films without vacuum break.

In this paper, we report an alternative route for the formation of such lower resistivity tungsten polycide interconnects by the amorphization of conventional tungsten polycide using a simple implantation technique. The conventional silicide is defined as a stand-alone process consisting of the formation of a doped poly-Si layer, HF cleaning for removal of the native oxide on the poly-Si surface, and the deposition of the DCS-WSi_x film. It was found that the DCS-WSi_x film was easily amorphized during implantation and the large-grain WSi_x was formed following thermal treatment, resulting in lowering of resistivity to 30% that of conventional polycide. In addition, no adverse effects to device performance were observed, and the properties of line resistance and dopant depletion effect improved.[21] This systematic study reviews the interaction of the silicide structure, the implantation conditions, and the electrical properties of a quarter-micron device.

Experimental

Oxidized 8 in. Si wafers were used as the substrate. In situ doped poly-Si films, 100 and 50 nm thick, were deposited using a commercial tubular-type low-pressure chemical vapor deposition (LPCVD) system in which the phosphorus concentration was about 4.5×10^{20} cm^{-3}. After HF dip, the DCS-WSi_x films were deposited using a commercial LPCVD reactor (Applied Materials, Centura) at 570°C and 0.9 Torr. The flow rate of DCS and WF_6 was maintained at 175 and 4 sccm, respectively. By Rutherford backscattering spectroscopy (RBS)[10] it was found that the atomic ratio (x) of the silicide was 2.6 (i.e., $WSi_{2.6}$) and fairly uniform in depth. During the deposition, the thickness of the silicide was controlled at 100 and 150 nm for a total polycide thickness of 200 nm, as shown in Table I.

After policide formation, phosphorus, arsenic, boron, or argon ions were implanted to the polycide with doses ranging from $1 \times$

Table I. Process split used.

Split name	Structure	Implantation
split 1	WSi_x (100 nm)/poly-Si (100 nm)	No
split 2	WSi_x (100 nm)/poly-Si (100 nm)	Yes
split 3	WSi_x (150 nm)/poly-Si (50 nm)	No
split 4	WSi_x (150 nm)/poly-Si (50 nm)	Yes

10^{15} to 8×10^{15} cm^{-2}. After implantation, transport of ion matter (TRIM) simulation[22] was made in an effort to quantify the as-implanted profiles of the ions in the polycide. Following simulation, thermal annealing was performed using a conventional furnace at 900°C for 30 min in a nitrogen ambient.

The thickness of the films was determined by cross-sectional scanning electron microscopy (SEM, Hitachi S5000). The identification of the silicide phases and the chemical status of the silicide surface were performed using X-ray diffraction (XRD, Mac Science M18XHF-22) and X-ray photoelectron spectroscopy (XPS, VG Escalab 220iXL).[23] The silicide structure was characterized primarily using a field emission gun transmission electron microscope (FEG-TEM, Philps CM200-FEG). The surface morphology of the films was quantified using atomic force microscopy (AFM, Park Science, Autoprobe M5). The sheet resistance of the films was measured using a four-point probe.

In order to evaluate the polycide as a conductor, a quarter-micron design rule CMOS was fabricated using a conventional fabrication procedure except for the formation of the gate electrodes, as shown in Table I. Here splits 1 and 3 indicate the conventional structured polycide, and splits 2 and 4 the implanted polycide. It is noted that after the thermal activation (i.e., 900°C, 30 min), three additional

thermal cycles at 850°C for 30 min in an N$_2$ ambient were applied to simulate the real fabrication of a DRAM device.

Results and Discussion

Structural and electrical changes of the silicide due to ion implantation.—Most of those studies were carried out with the phosphorus implantation of the polycide having the structure of DCS-WSi$_x$ (150 nm)/poly-Si (50 nm), i.e., splits 3 and 4. Results with other implantation species, such as boron, arsenic, and argon, are discussed in Fig. 14-17.

The distribution of the ion-implanted atoms in the polycide were simulated using TRIM, as shown in Fig. 1a. The projected ranges were calculated to be 33, 47, 62, 76, and 90 nm for implantation energies of 40, 60, 80, 100, and 120 keV, respectively. It was found that with implantation energies above 100 keV, the tail of the distribution was in the underlying poly-Si layer, and the atoms penetrated the underlying poly-Si, 50 nm thick, when the energy reached 120 keV. Figure 1b shows the structural change of the silicide as a function of the implantation energy with a fixed dose of 5×10^{15} cm^{-2}. In the case of the unimplanted silicide (i.e., split 3), a typical crystalline spectrum of hcp-WSi$_2$ was observed, as described elsewhere.[6,8,10,11] The ion implantation, even with the lowest energy of 40 keV, resulted in a drastic decrease of the diffraction peak intensities. In addition, the intensities were further decreased with increasing energy. When the energy exceeded over 100 keV, at which point the tail of the distribution is within the underlying poly-Si, the diffraction peaks became broad. This clearly suggests that the DCS-WSi$_x$ film is amorphized by the ion implantation, and the fraction of the amorphized layer strongly depends on the implantation energy.

Considering the gate oxide degradation due to metallic contamination induced by metal knock-on effect, the implantation energy should be controlled to retain most of the atoms within the silicide. As an example, for a 150 nm thick DCS-WSi$_x$ layer, the maximum energy would be 80. The effect of the energy dependence on the gate oxide integrity was verified and is discussed in Fig. 10 and 11. For the structure of WSi$_x$ (100 nm)/poly-Si (100 nm), split 1 and 2, the corresponding energy should be 50 keV, as reported in Ref. 21.

Figure 2 shows the cross-sectional TEM image of a sample from split 4 after implantation (P$^+$, 5×10^{15} cm^{-2}, 80 keV), exhibiting the amorphization of the silicide except for a polycrystalline layer at the silicide/poly-Si interface. The weaker peak intensity of hcp-WSi$_2$ shown in Fig. 1b is due to this layer. The remaining crystallites could be explained by the previous TRIM simulation [Fig. 1a]; at that implantation condition, most of phosphorus atoms are contained
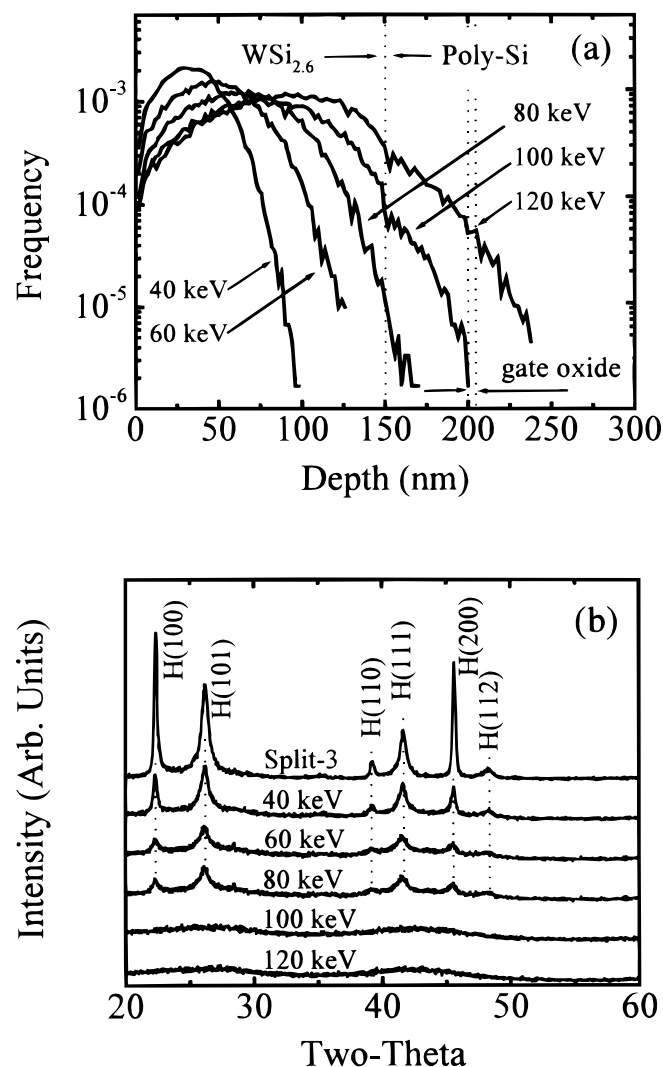

Figure 1. (a) TRIM simulated distributions of phosphorous atoms in the polycide as a function of implantation energy. (b) XRD spectra of the polycide showing the structural change according to the implantation energy in which "H" means hcp-WSi$_2$.
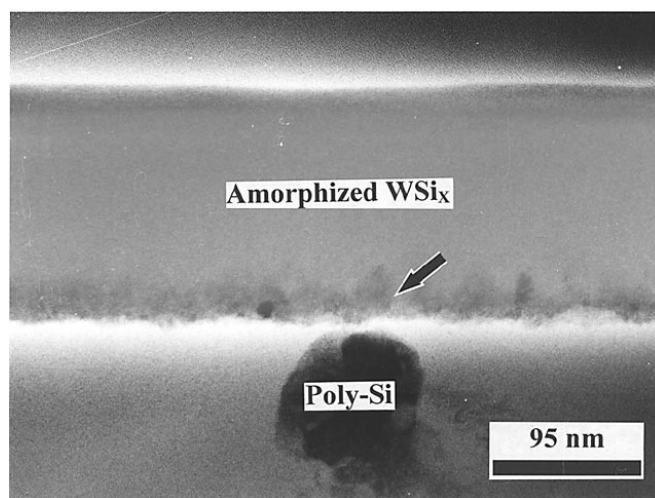
Figure 2. Cross-sectional TEM image of a sample from split 4 after phosphorous implantation (5×10^{15} cm^{-2} and 80 keV) showing amorphization of the silicide. The remnant crystallite at the interface is indicated by an arrow.
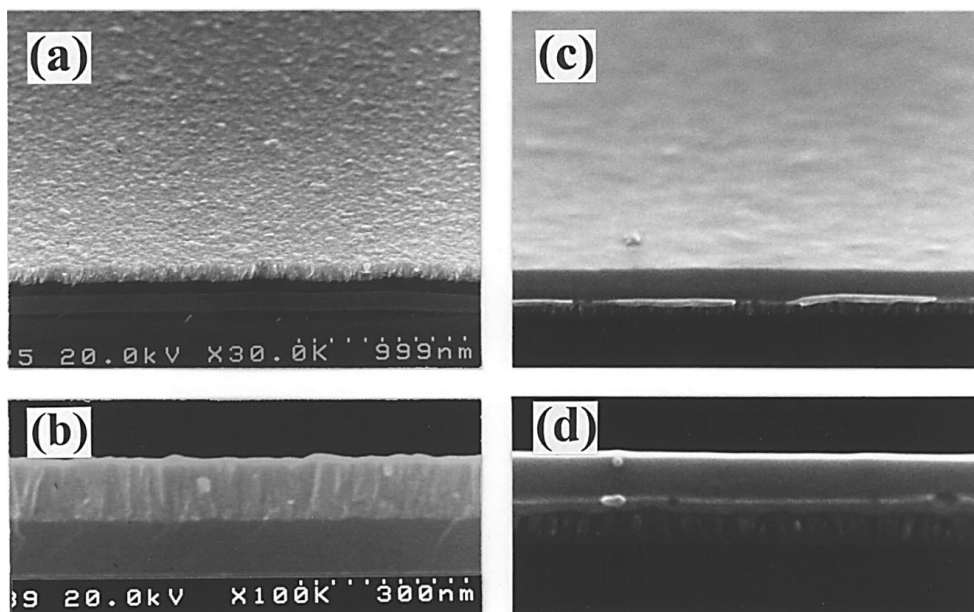
Figure 3. SEM image of silicide showing the morphology according to the implantation: (a) tilted and (b) cross-sectional view of split 3; (c) tilted and (d) cross-sectional view of split 4.

within the silicide, since the projected range is 62 nm, so that the number of atoms in the silicide close to the interface is not enough to amorphize the silicide. Such an amorphization also resulted in a drastic change of surface morphology, as shown in Fig. 3; after the implantation, the polycrystalline surface with columnar structure of unimplanted DCS-WSi$_x$ [8] was modified to a smooth surface with no apparent grains. At that time, average root mean square (rms) values from AFM measurement give 1.99 and 0.97 nm, respectively, which is discussed again in Fig. 9.

Figure 4 shows the variation of sheet resistance as a function of implantation energy. The sheet resistance decreases with increasing energy. Above 100 keV, the point at which the entire silicide layer is amorphous according to Fig. 1b, the resistance comes to saturation. This means that the sheet resistance is related to the fraction of amorphized silicide. As a consequence, the sheet resistance decreases with increasing fraction of amorphized layer.

Figure 5 shows the dependence of peak intensities and sheet resistance on the implantation dose in which the implantation energy was fixed at 80 keV. When the dose is increased, the peak intensity of the remaining hcp-WSi$_2$ crystallite was decreased with a con-

current reduction in sheet resistance. Such an observation could be explained as follows the increase of dose does not result in a change of the projected range but rather in an increase in the number of
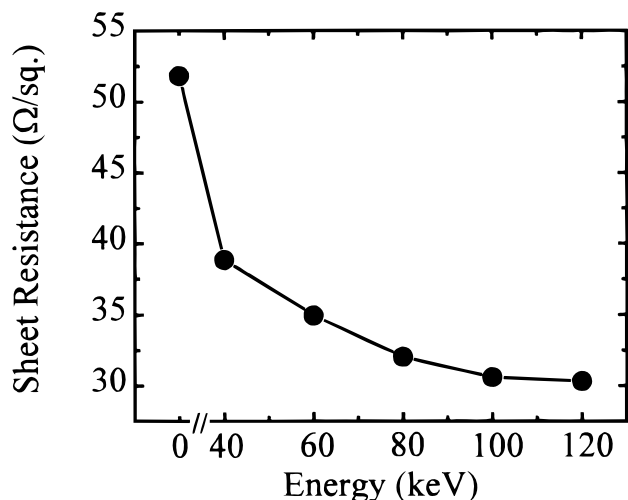

Figure 4. Sheet resistance variation of split 4 as a function of the condition of implantation. The phosphorus ions were implanted with varying the energy from 40 to 120 keV at a fixed dose of 5×10^{15} cm^{-2}.

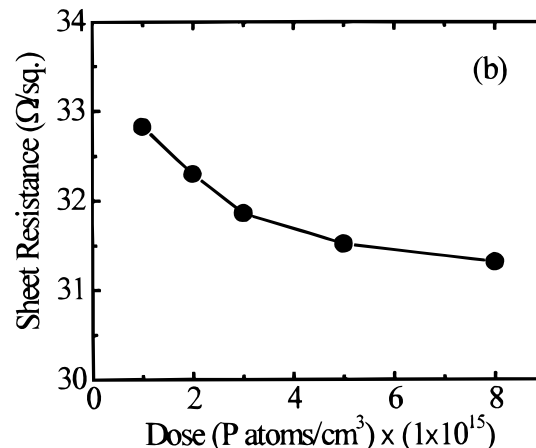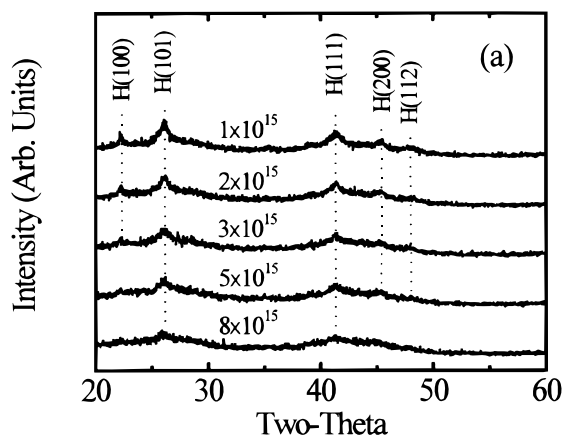**Figure 5.** Variation of (a) XRD peak intensities and (b) sheet resistance of split 4 as a function of the dose from 1×10^{15} to 8×10^{15} cm^{-2} at fixed energy of 80 keV.
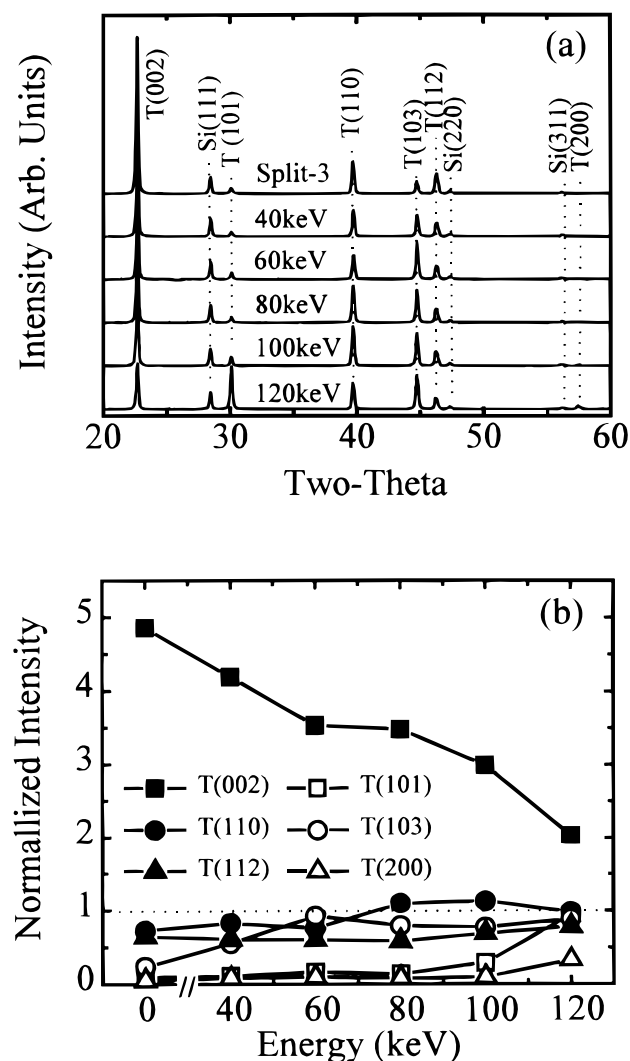
Figure 6. (a) XRD spectra and (b) normalized peak intensity of the same samples shown in Fig. 1 after thermal annealing at 900°C for 30 min in N_2 ambient. "T" means tet-WSi_2.

Figure 7. Sheet resistance variation of split 4 after thermal annealing: the phosphorous ions were implanted with variation of (a) energy ranging 40-120 keV at fixed dose of 5×10^{15} cm^{-2} and (b) dose from 1×10^{15} to 8×10^{15} cm^{-2} at fixed energy of 80 keV.

implanted atoms which is needed for amorphization, especially at the interface, so that that the fraction of amorphization is increased.

Structural and electrical change of the silicide according to thermal annealing.—As previously mentioned, the silicide films were transformed into tet-WSi_2 after the thermal annealing, as shown in Fig. 6a. Interestingly, it appeared that the relative peak intensity of each diffraction plane was varied with the implantation energy; unimplanted silicide (i.e., split 3), for example, is highly textured along the orientation of (002) tet-WSi_2. For the implanted silicide, the intensity of the (002) plane was decreased with increasing energy, while the intensities of the other planes were fairly constant.

In order to quantify this trend, the normalized peak intensity of each condition was calculated as a function of the energy, as shown in Fig. 6b. Here the normalized intensity was defined as the fraction of each peak intensity with respect to the summation of all peak
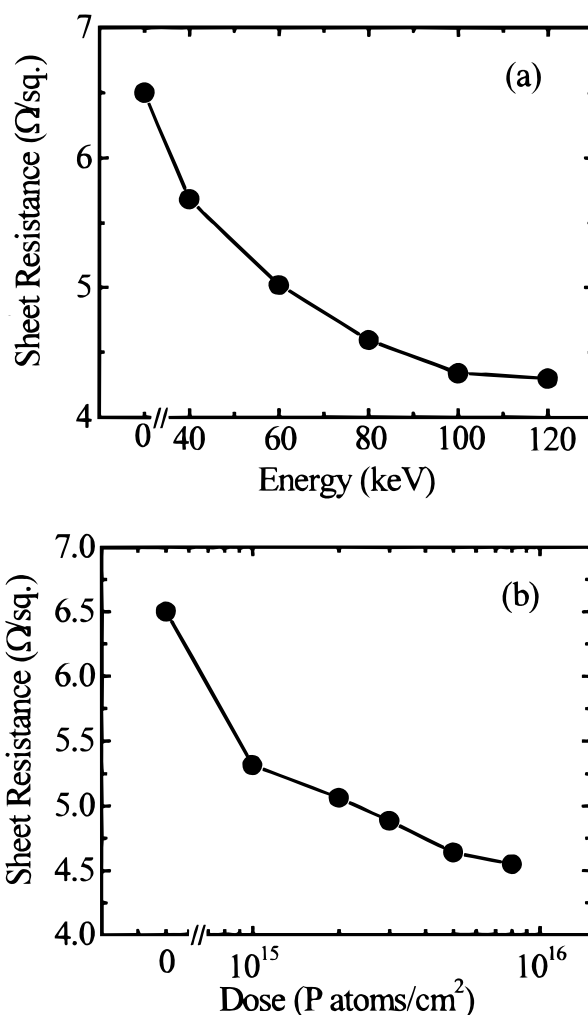
intensities, which was again divided by the standard powder diffraction intensity from the JCPDS database.[13,24] In this figure, the intensity corresponding to the standard powder diffraction intensity is indicated by a dotted line. For the unimplanted silicide (i.e., split 3), a highly preferred texture of (002) tet-WSi_2 was observed (Fig. 6a). With increasing energy, the normalized intensity of each plane approached that of powder diffractometry (i.e., random oriented reflection). This finding suggests the dependence of recrystallization of tet-WSi_2 on the hcp-WSi_2.[14] In fact, the strong structural correlation between the (100) plane of hcp-WSi_2 and the (002) plane of tet-WSi_2[11,13] results in the preferred texture of the (002) tet-WSi_2, which also restricts the grain growth of the tet-WSi_2. Since the implantation dislodges the atoms in the silicide, the effect of the hcp-WSi_2 on the nucleation and grain growth is diminished with increasing fraction of amorphized layer. Therefore the sheet resistance (i.e., resistivity) of the silicide depends upon the implantation conditions

Table II. Variation of resistivity as a function of implantation energy after thermal annealing in which the implantation dose was fixed at 5×10^{15} cm^{-2}.

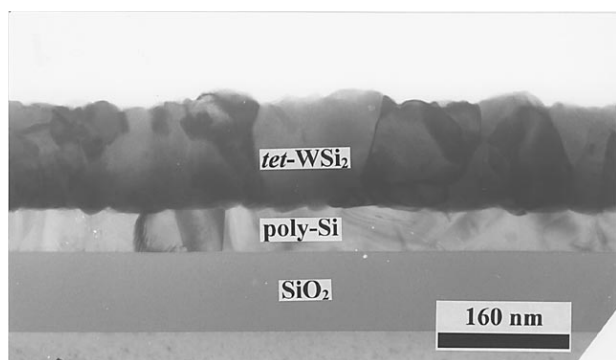| Energy (keV)	0	40	60	80	100	120
Resistivity ($\mu\Omega$ cm)	97.5	85.2	75.3	68.8	65.1	64.5
Resistivity lowering (%)	0	−12.6	−22.8	−29.4	−33.2	−33.8

Figure 8. Cross-sectional TEM images of polycide (split 4; phosphorous implantation at 5×10^{15} cm^{-2} and 80 keV) after thermal annealing at 900°C for 30 min in N$_2$ ambient.

(e.g., energy and dose), which determines the amorphization fraction of silicide, as shown in Fig. 7 and Table II. The resistivity of silicide is decreased with increased energy or dose. It was found that the resistivity was lowered about 30% in comparison with that of unimplanted silicide when the energy was above 80 keV.

As evidence for this explanation, a cross-sectional image of implanted and annealed silicide (split 4) is shown in Fig. 8. Contrasted to the unimplanted silicide,[8,14] the implantation resulted in a smoother surface even after thermal annealing, as shown in Fig. 9. The rms values from AFM of the unimplanted silicide (i.e., split 3) were measured to be 1.99 and 1.91 nm before and after thermal annealing, respectively, while that of the implanted silicide (i.e., split 4) 0.97 and 0.93 nm, respectively. Such an observation of lower rms value is attributed to the formation of larger grains from the amorphized silicide, which is an advantage for future fabrication processes, photolithography in particular.

Electrical characterization of the silicide as a gate electrode.— Figure 10 shows quasi-static and high-frequency capacitance-voltage (C-V) characteristics of the polycide as a gate electrode, where the implantation energy was varied from 60 to 120 keV with the dose fixed at 5×10^{15} cm^{-2}. One interesting fact worth reporting here is the dopant depletion effect occurring in unimplanted silicide (i.e., split 3). The effect is attributed to the diffusion of dopant into the upper silicide layer from the underlying poly-Si layer during high-temperature processing, the so-called dopant depletion effect.[25] The dopant loss occurs because impurity diffusion coefficients in silicide are larger by several orders of magnitude than in silicon, which may effect device performance.[26,27] Since the capacitance of the inversion region (C_{INV}) is a strong function of the extent of the dopant depletion in the gate electrode, the ratio of C_{INV} to the capacitance in the accumulation region (C_{OX}) (i.e., C_{INV}/C_{OX}) could be used as the gate depletion index of the gate electrode. In this case, the C_{INV}/C_{OX} was calculated to be 0.82 at bias voltage of 4.5.

At implantation energies less than 80 keV, the C_{INV}/C_{OX} increased to 0.96. This is because during thermal annealing the dopant loss from the poly-Si was compensated for by diffusion from the upper silicide. Implantation with higher energy (100 keV) results in threshold voltage shifts and the degradation of C_{INV}/C_{OX}. According to the TRIM simulation (not shown here), many metallic atoms (e.g., tungsten) recoil into the poly-Si due to the metal knock-on effect.[28] From this it is inferred that degradation is due to the metallic contamination of the gate oxide. At the highest energy of 120 keV, moreover, not only a threshold voltage shift was observed but the dopant also penetrated toward the substrate, which was predicted from the TRIM simulation shown in Fig. 1a.

Figure 11 compares the time-dependent dielectric breakdown (TDDB) of the gate electrode as a function of implantation energy. The failure rate was found to be nearly the same as that of the unimplanted polycide (i.e., split 3) if the energy is less than 80 keV. When the energy is increased to over 80 keV (e.g., 100 and 120 keV), the
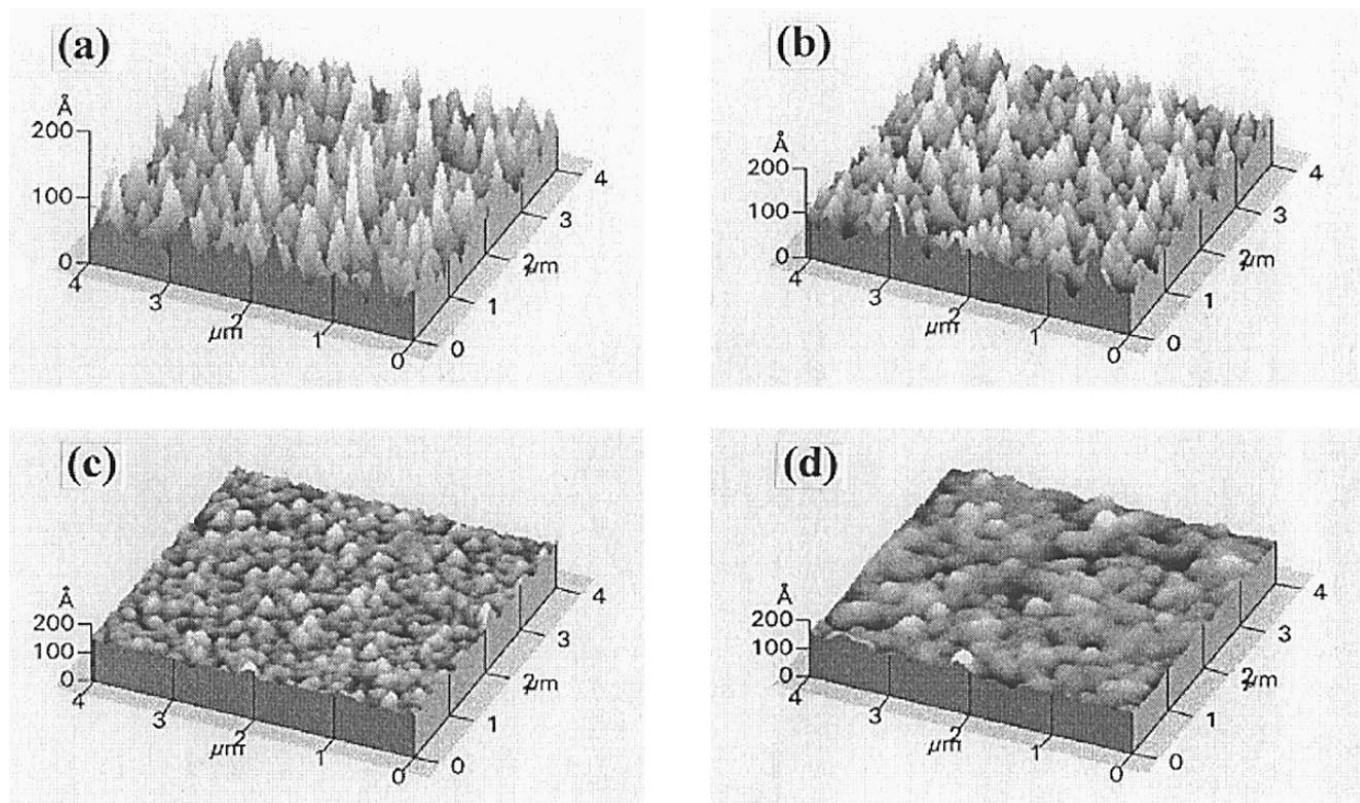

Figure 9. AFM images of the polycide. Split 3: (a) as-deposited and (b) after thermal annealing; split 4: (c) as-deposited and (b) after thermal annealing. Implantation performed at 5×10^{15} cm^{-2} and 80 keV.

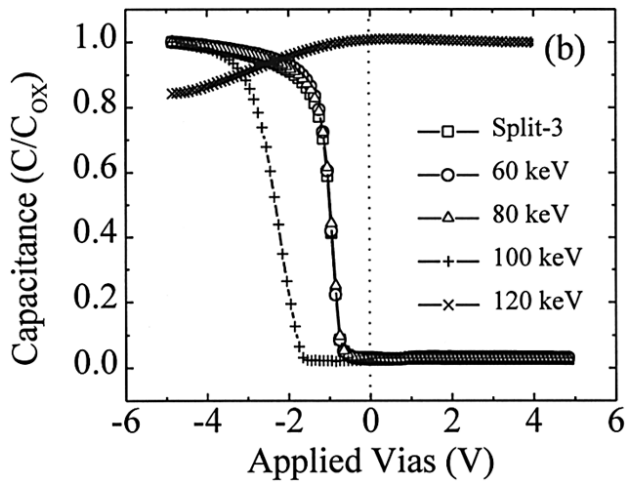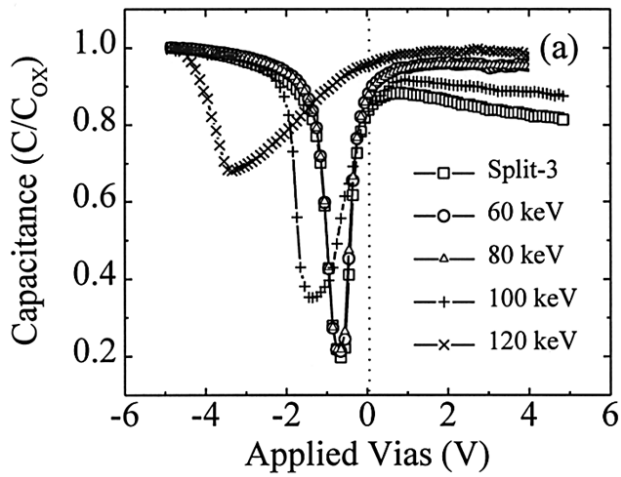**Figure 12.** Cross-sectional TEM of a split 4 sample showing the structure of the polycide at the active area/isolation interface.

ple was very stable and uniform, even at the valley formed between the oxide isolation and the active area.

Figure 13a shows the variation of sheet resistance as a function of linewidth of the gate electrode of split 1-4. For linewidths ranging 0.25-10.0 µm, the sheet resistance of the phosphorus-implanted polycides (i.e., split 2 and 4) was about 30% lower than that of the

Figure 10. (a) Quasi-static and (b) high-frequency C-V characteristics of gate electrode as a function of implantation energy.

failure rate increased due to metallic contamination and dopant penetration, which is consistent with the C-V characterization.

In Fig. 12, the cross-sectional view of the device used in this experiment is shown. It was found that the structure of a split 4 sam-
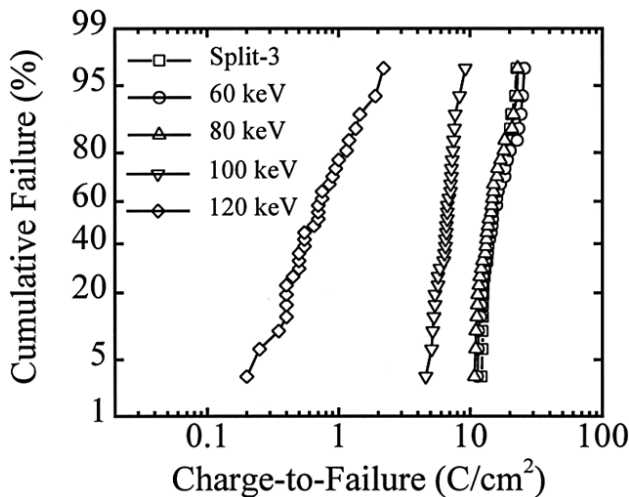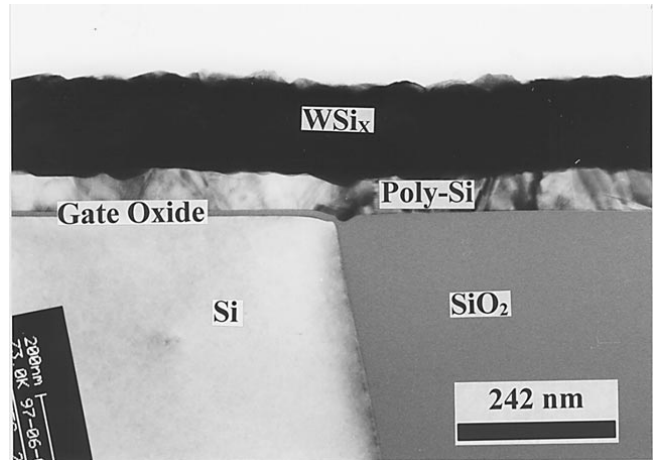

Figure 11. TDDB characteristics of gate electrode as a function of implantation energy.
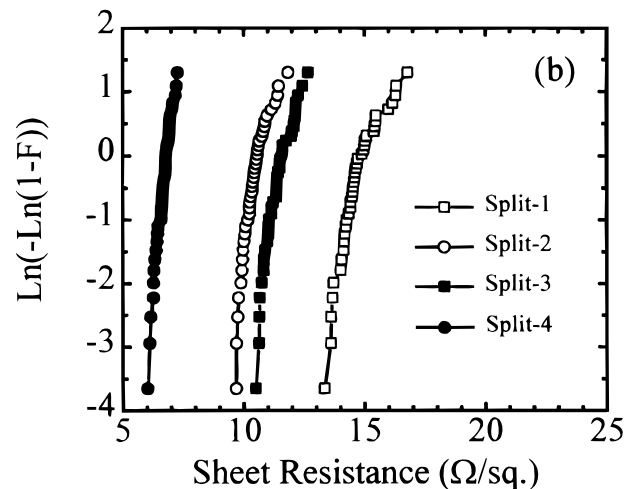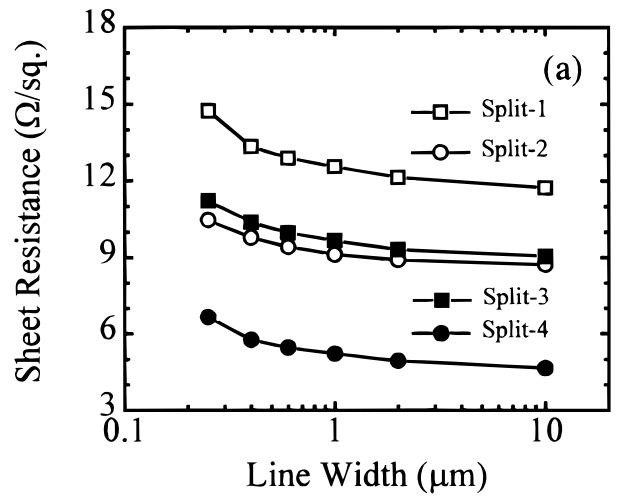

Figure 13. (a) Linewidth dependence and (b) distribution of gate resistance.
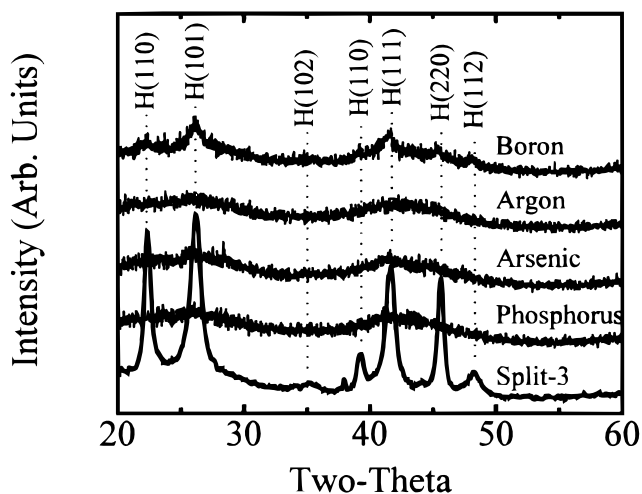
Figure 14. XRD spectra of split 4 samples: as-deposited (split-3) and after implantation of P (100 keV), As (220 keV), Ar (120 keV), and B (35 keV), in which the doses were fixed at 5×10^{15} cm^{-2}.
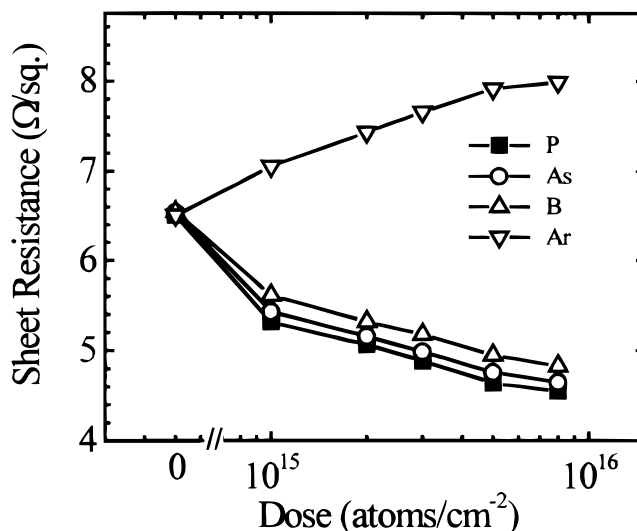

Figure 15. Sheet resistance variation of split 4 as a function of implantation dose and species in which the sheet resistance was measured after thermal activation.

unimplanted polycides (i.e., split 1 and 3) due to the decrease of the WSi$_x$ resistivity shown in Fig. 7 and Table II. At the minimum linewidth of 0.25 μm, the line resistance of splits 1, 2, 3, and 4 was measured to be 14.73, 10.46, 11.22, and 7.56 Ω/□, respectively, which was averaged over 49 points per wafer. A comparison of the distribution line resistance at 0.25 μm is shown in Fig. 13b. From these results it can be concluded that the implantation of phosphorus with energies less than 80 keV (50 keV in case of 100 nm thick silicide)[21] improves electrical performance, such as line resistance and dopant depletion effect, with no adverse effects on other device characteristics. This suggests that the amorphization technique is a convenient choice for the electrode formation, such as gate and bit-line, for future devices.

Effect of implantation species.—We performed similar experiments using other implantation species such as boron, argon, and arsenic. The implantation energy was determined by TRIM simulation for the projected range to be located around the center of 150 nm thick DCS-WSi$_x$, 40, 120, 220, and 100 keV for boron, argon, arsenic, and phosphorus ions, respectively. During the implantation the doses were fixed at 5×10^{15} cm^{-2}.

Figure 14 illustrates the XRD reflections after the implantation, with unimplanted silicide shown for comparison. The DCS-WSi$_x$ was easily amorphized even by implantation using the lightest species, such as boron. A feasible cause of the amorphization of

DCS-WSi$_x$ is likely its specific crystalline feature, a feather-fine columnar structure with weak chemical binding.[8,14] Implantation with even the lightest ions (e.g., boron) easily dislodges the atoms, resulting in amorphization.

Figure 15 shows the dependence of sheet resistance on the implantation species and dose. It was found that boron, arsenic, and phosphorus showed similar dependencies as shown in Fig. 7b, and that the sheet resistance from the phosphorus-implanted silicide was the lowest among all species. In the case of argon implantation, however, it appeared that the sheet resistance increased with increasing dose.

To investigate further, the morphology of thermally annealed silicides was examined by SEM, as shown in Fig. 16. The surface was fairly uniform, as expected from Fig. 9. A mound was observed on the surface of boron-implanted silicide, which is discussed again in Fig. 17. In the argon-implanted silicide, a high density of voids appeared at the surface and in the bulk of the film. It is speculated that the implanted argon migrates to form a void in the film during thermal annealing, since argon is chemically inert. Therefore, the density and size of the voids due to the argon are increased with increasing dose, which may result in the decrease of grain size and the increase of sheet resistance.

In order to characterize the chemical status of the surface, XPS was performed on the samples, as shown in Fig. 17. The XPS was
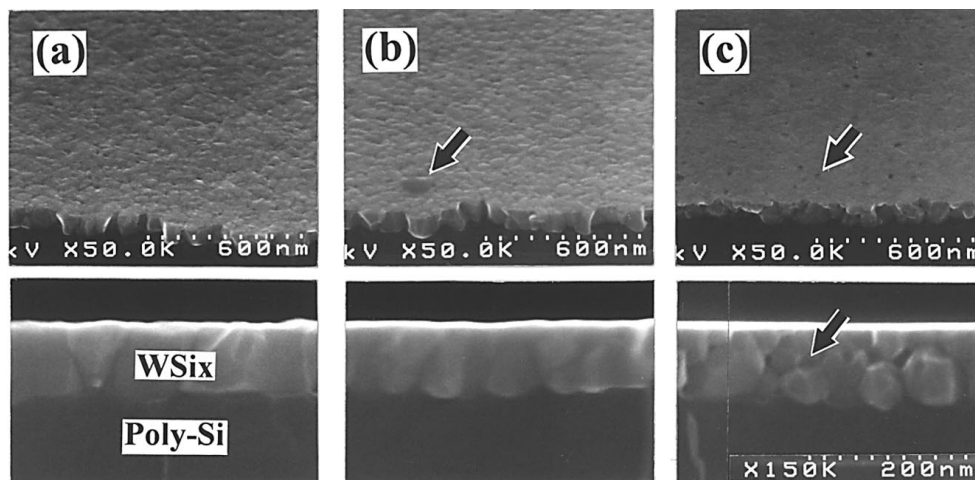

Figure 16. SEM micrographs of the polycide samples after thermal annealing: (a) phosphorus (100 keV), (b) boron (35 keV), and (c) argon (120 keV) were implanted with fixing the dose at 5×10^{15} cm^{-2}. A compound on the surface, in (b), and voids in the silicide film, in (c), are marked by arrows.
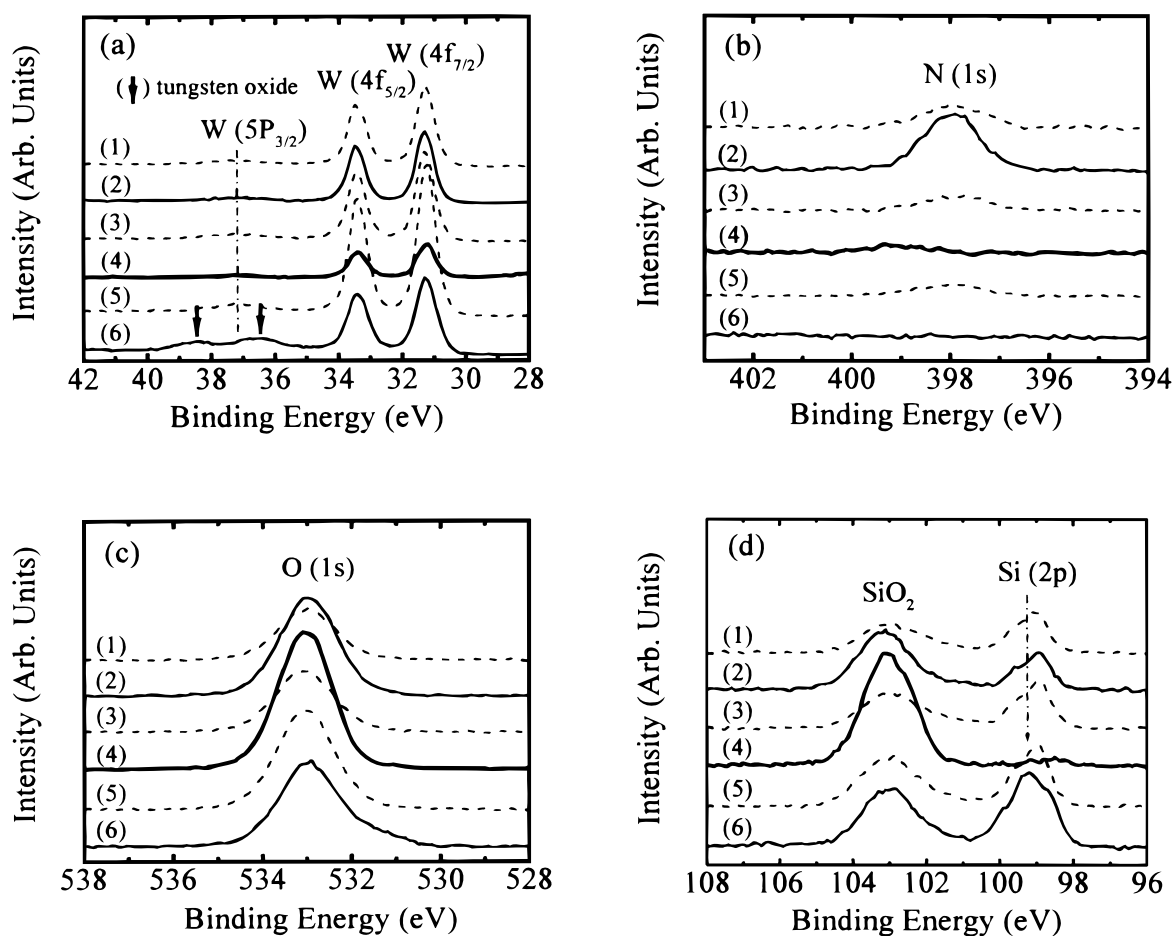
Figure 17. XPS spectra showing the binding energy shifts of (a) W, (b) N, (c) O, and (d) Si in which (1), (2), (3), and (4) indicate the argon-, boron-, arsenic-, and phosphorus-implanted samples, and (5) and (6) are thermal-treated and as-deposited split 3 samples.

carried out without surface treatment (i.e., sputter etching), and each peak was normalized by the binding energy of the absorbed carbon peak (C_{1s}) at 284.5 eV. For comparison, as-deposited and thermally annealed unimplanted silicides (split 3) were used as control samples.

From the binding energy shift of silicon (Si 2P, Fig. 17d) it is known that the as-deposited silicide has significantly large amounts of free silicon atoms, which might be due to the excessive silicon in the silicide (i.e., $WSi_{2.6}$). After thermal annealing, that peak disappears while the peak due to silicide formation increases in size. The binding energy shift due to tungsten oxide (Fig. 17a) also disappeared at the surface of the as-deposited silicide. Upon annealing, these peaks could no longer be observed. This indicates that a native oxide layer consisting of silicon oxide and tungsten oxide is formed during air exposure at the surface of as-deposited silicide film. Upon thermal annealing, the surface layer is covered by silicon oxide, that is, a capping oxide, which implies that the excessive silicon atoms from the bulk of as-deposited silicide diffuse to the surface to form a silicon oxide.[8,29]

An interesting observation from the boron-implanted silicide is the intensity of the nitrogen peak, which is the strongest nitrogen peak among all the samples. This implies that boron nitride may be formed during the thermal anneal in the N_2 ambient. Although not shown here, a strong binding energy shift of boron due to the formation of boron nitride was observed at about 188 eV,[23] which supports the implication.

As for the phosphorus-implanted samples, it was found that the intensity of tungsten was the weakest while that of oxygen the strongest. Moreover, the binding energy shift of silicon due to the formation of silicon oxide (~103 eV) was observed while that of sil-

icon, Si (2p) at about 99.2 eV was not. These results suggest that relatively thicker silicon oxide was formed at the surface of the phosphorus-implanted silicide. At this time, the driving force for this phenomenon is not fully understood. In the case of the phosphorus-implanted silicide, the excess silicon atoms in the silicide are the ones most effectively outdiffused toward the surface during thermal annealing, which might be expected to affect the grain growth of tet-WSi_2 with a concomitant reduction of the sheet resistance of the polycide layer.[29,30]

Conclusion

1. As-deposited DCS-WSi_x is easily amorphized by implantation. The fraction of an amorphized layer is dependent on the implantation conditions, such as energy and dose. After thermal annealing, the sheet resistance (or resistivity) is decreased with increasing implantation energy and dose, and reduced to 30% that of unimplanted silicide.

2. The grain size of recrystallized tet-WSi_2 from amorphized silicide is larger than that from as-deposited hcp-WSi_2, which results in a smoother surface and lower resistivity.

3. When the implantation energy is controlled so that the ion is contained within the silicide, the electrical properties of the device are not adversely affected. Additionally, the dopant depletion effect is improved by compensation of the dopant loss from the underlying poly-Si.

4. The line resistance of phosphorous-implanted silicide is about 30% lower than that of unimplanted silicide even after device fabrication.

5. Among all implantation species, phosphorus was found to be the most effective in lowering the resistivity. Although argon implantation results in amorphization, the resistivity is increased with increasing dose due to the formation of voids in the silicide film.

Acknowledgments

The authors thank J. T. Choi, K. W. Kim, S. B. Yon, and the Analytical Technology Department of LG Semicon Company, Limited, for their kind support in the analytical works, and Bart van Schravendijk, Patrice Garaghty, and Richard Swope of Novellus Systems, Incorporated, for their useful discussions and encouragement.

References

1. G. Giroult, A. Nouailhat, and M. Gauneau, *J. Appl. Phys.*, **67**, 515 (1990).
2. T. Hara, T. Miyamoto, and T. Yokoyama, *J. Electrochem. Soc.*, **136**, 1177 (1989).
3. K. Shenai, *IEEE Trans. Electron Devices*, **ED-39**, 193 (1992).
4. Y. W. Kim, N. I. Lee, and M. H. Park, *Mater. Res. Soc. Symp. Proc.*, **355**, 491 (1995).
5. J. B. Price, J. Wu, Y. Chow, and J. Mendoca, *Semicon West*, May 10, 1986.
6. T. Hara, T. Miyamoto, H. Hagiwara, E. I. Bromley, and W. R. Harshbarger, *J. Electrochem. Soc.*, **137**, 2955 (1990).
7. J. T. Hillman, W. M. Triggs, and M. Aruga, *J. Electrochem. Soc.*, **139**, 3574 (1992).
8. S. G. Telford, M. Eizenberg, M. Chang, A. K. Sinha, and T. R. Gow, *J. Electrochem. Soc.*, **140**, 3689 (1993).
9. S. G. Telford, M. Eizenberg, M. Chang, A. K. Sinha, and T. R. Gow, *Appl. Phys. Lett.*, **62**, 1766 (1993).
10. J. S. Byun, B. H. Lee, J.-S. Park, and J. J. Kim, *J. Electrochem. Soc.*, **144**, 3572 (1997).
11. M. d'Heurle, C. S. Peterson, and M. Y. Tsai, *J. Appl. Phys.*, **51**, 5796 (1980).
12. M.-A. Nicolet and S. S. Lau, in *VLSI Electronics: Microstructure Science*, Vol. 6, N. G. Einspruch and G. B. Larrabee, Editors, Academic Press, New York (1983).
13. JCPDS, 11-915, International Center for Diffraction Data, Swarthmore, PA.
14. J. S. Byun, B. H. Lee, J.-S. Park, D. K. Sohn, S. J. Choi, and J. J. Kim, *J. Electrochem. Soc.*, **145**, 3228 (1998).
15. Y. Akasaka, S. Suehiro, K. Nakajima, T. Nakasugi, K. Miyano, K. Kasai, H. Oyamatsu, M. Kinugawa, M. T. Takaki, K. Agawa, F. Matsuoka, M. Kakumu, and K. Suguro, *IEEE Trans. Electron Dev.*, **ED-43**, 1864 (1996).
16. M. T. Takaki, K. Miyashita, H. Koyama, K. Nakajima, K. Miyano, Y. Akasaka, Y. Hiura, S. Inaba, A. Azuma, H. Koike, H. Yoshimura, K. Suguro, and H. Ishiuchi, *Tech. Dig. Int. Electron Devices Meet.*, 455 (1996).
17. H. Wakabayashi, T. Andoh, K. Sato, K. Yoshida, H. Miyamoto, T. Mogami, and T. Kunio, *Tech. Dig. Int. Electron Devices Meet.*, 447 (1996).
18. K. A. Jenkins, J. N. Burghart, P. D. Agnello, D. F. Heidel, and C. Y. Wong, *Tech. Dig. Int. Electron Devices Meet.*, 891 (1993).
19. D. L. Bae, E. H. Lee, H. S. Kim, G. H. Choi, D. H. Ko, H. K. Kang, and M. Y. Lee, *Proceedings of the ULSI Multilevel Interconnection Conference, VMIC*, p. 521-523 (1996).
20. J. S. Byun, J.-S. Park, B. H. Lee, D. K. Sohn, J. W. Park, J. J. Kim, and J. M. Hwang, *Tech. Dig. Int. Electron Devices Meet.*, 119 (1997).
21. J. S. Byun, B. H. Lee, J.-S. Park, D. K. Sohn, and J. J. Kim, Extended Abstracts of the 1997 International Conference on Solid State Devices and Materials (SSDM), p. 282, Hamamtsu, Japan (1997).
22. J. F. Ziegler, J. P. Biersack, and U. Littmark, *The Stopping and Range of Ions in Solids*, Pergamon Press, New York (1985).
23. J. F. Moulder, W. F. Stickle, P. E. Sobol, and K. D. Bomben, *Handbook of X-Ray Photoelectron Spectroscopy*, J. Chastain, Editor, Perkin-Elmer, Eden Prairie, MN (1992).
24. B. D. Culity, *Elements of X-Ray Diffraction*, 2nd ed., Addison-Wesley Publishing Co., Reading, MA (1978).
25. T. Hosoya, K. Michida, K. Imai, and E. Arai, *IEEE Trans. Electron Devices*, **ED-42**, 2111 (1995).
26. H. Hayashida, Y. Toyojima, Y. Suizu, K. Mitsuhashi, H. Iwai, and K. Maeguchi, *Tech. Dig. VLSI Symp.*, 29 (1992).
27. C. L. Huang and N. D. Arora, *IEEE Trans. Electron Devices*, **ED-40**, 2330 (1993).
28. Q. Wang, C. M. Osburn, and C. A. Canovai, *IEEE Trans. Electron Devices*, **ED-39**, 2486 (1992).
29. R. Palman, B. Vermeire, and K. Maex, *Mater. Res. Soc. Symp. ULSI-IX*, 489 (1994).
30. C. M. Ting, *Tech. Dig. Int. Electron Devices Meet.*, 110 (1980).